Mon. Not. R. Astron. Soc. **371,** 1503–1512 (2006) doi:10.1111/j.1365-2966.2006.10787.x

Predicted properties of RR Lyrae stars in the Sloan Digital Sky Survey photometric system

M. Marconi,[1⋆] M. Cignoni,[1] M. Di Criscienzo,[1,2] V. Ripepi,[1] F. Castelli,[3] I. Musella[1] and A. Ruoppo[1,4]

[1]*INAF-Osservatorio Astronomico di Capodimonte, Via Moiarello 16, I-80131, Napoli, Italy*
[2]*Università di Torvergata, Via della Ricerca Scientifica 1, 00133 Roma, Italy*
[3]*INAF-Osservatorio Astronomico di Trieste, via Tiepolo 11, 34131 Trieste, Italy*
[4]*Università Federico II, Complesso Monte S.Angelo, 80126 Napoli, Italy*

Accepted 2006 July 8. Received 2006 June 28; in original form 2006 May 15

ABSTRACT

The luminosities and effective temperatures, as well as the whole bolometric light curves of non-linear convective RR Lyrae models with $0.0001 \leqslant Z \leqslant 0.006$, are transformed into the Sloan Digital Sky Survey (SDSS) photometric system. The obtained *ugriz* light curves, mean magnitudes and colours, pulsation amplitudes and colour–colour loops are shown and analytical relations connecting pulsational to intrinsic stellar parameters, similar to the ones currently used in the Johnson–Cousins filters, are derived. Finally, the behaviour in the colour–colour planes is compared with available observations in the literature and possible systematic uncertainties affecting this comparison are discussed.

Key words: stars: horizontal branch – stars: variables: other.

1 INTRODUCTION

Among Population II radially pulsating stars, RR Lyrae play a relevant role both as standard candles and as stellar property tracers. They are bright stars, easily identified thanks to their characteristic variability (light curves, periods and colours) and their luminosity spans a narrow range. They usually show low ($Z \sim 0.0001$) to intermediate ($Z \sim 0.006$) metallicity, but they can reach solar abundances in the solar neighbourhood or in the Galactic bulge. The calibration of their absolute magnitude $M_V(RR)$ in terms of the measured iron-to-hydrogen content [Fe/H] allows us to use these variables to infer the distances of Galactic Globular Clusters (GGC) and nearby galaxies, as well as to calibrate secondary distance indicators such as the globular cluster (GC) luminosity function (see Di Criscienzo et al. 2006 and references therein). In this context, several observational and theoretical efforts have been made in the last few years to provide accurate evaluations of the $M_V(RR)$–[Fe/H] relation, usually approximated as $M_V(RR) = \alpha + \beta$[Fe/H] (see e.g. Caputo et al. 2000; Cacciari 2003, and references therein), and to derive relevant implications for the Population II distance scale and the age of globular clusters. The above characteristics make RR Lyrae superb probes of the old stellar populations, and studies of their pulsation properties have provided much of our present knowledge of the structure, kinematics and the metal abundance distribution of the halo. Moreover, they have been adopted in the recent literature as fundamental targets of surveys devoted to the identification of specific populations and galactic substructures (see e.g. Brown et al. 2004; Vivas et al. 2004; Wu et al. 2005, and references therein). In particular, the Sloan Digital Sky Survey (SDSS) for RR Lyrae (Ivezic et al. 2000) and the Quasar Equatorial Survey Team (QUEST) RR Lyrae survey (Vivas et al. 2001, 2004; Vivas & Zinn 2006) detected the tidal stream from the Sagittarius dSph galaxy and other density enhancements in the halo that may be other tidal streams, supporting the idea that RR Lyrae surveys are crucial to trace the merger history of the Milky Way. In the context of the Very Large Telescope (VLT) Survey Telescope (VST) Guaranteed Time Observations (GTO; see Alcalá et al. 2006), we have planned a survey (STREGA@VST; see Marconi et al. 2006) devoted at the exploration of the southern part of the Fornax stream (Lynden-Bell 1982; Dinescu et al. 2004) and the tidal interaction of the involved satellite galaxies and globular clusters with the Milky Way halo. To this purpose, RR Lyrae will be used as tracers of the oldest stellar populations through multi-epoch observations in the SDSS *g* and *i* filters. The comparison with theoretical period–luminosity–colour, period–luminosity–amplitude and Wesenheit relations (see e.g. Marconi et al. 2003; Di Criscienzo, Marconi & Caputo 2004, hereafter D04) will provide information on the individual distances and in turn on the spatial distribution of the investigated stellar system. In this context, the addition of multi-epoch *r* and single-epoch *u* exposures on selected fields will enable us to derive further constraints on the intrinsic stellar parameters of RR Lyrae stars. However, in order to correctly compare model predictions with observations, all the predicted pulsation observables need to be transformed into the SDSS photometric filters. To this purpose, in this paper we use updated model atmospheres to predict the pulsation properties

⋆E-mail: marcella@na.astro.it

Table 1. Model input parameters.

Z	Y	$M/M_\odot$	$\log L/\log L_\odot$
0.0001	0.24	0.65	1.61
0.0001	0.24	0.70	1.72
0.0001	0.24	0.75	1.61
0.0001	0.24	0.75	1.72
0.0001	0.24	0.75	1.81
0.0001	0.24	0.80	1.72
0.0001	0.24	0.80	1.81
0.0001	0.24	0.80	1.91
0.0004	0.24	0.70	1.61
0.0004	0.24	0.70	1.72
0.0004	0.24	0.70	1.81
0.001	0.24	0.65	1.51
0.001	0.24	0.65	1.61
0.001	0.24	0.65	1.72
0.001	0.24	0.75	1.61
0.006	0.26	0.58	1.55
0.006	0.26	0.58	1.65
0.006	0.26	0.58	1.75

of RR Lyrae stars of different metal contents in the u, g, r, i, z bands.[1]

This paper is organized as follows. In Section 2, we present the adopted pulsation models; in Section 3 we discuss the procedures adopted to transform the theoretical scenario into the SDSS filters and in Section 4 we illustrate the pulsation observables in these bands. Finally in Section 5, we compare model predictions with SDSS RR Lyrae data available in the literature, discussing possible systematic errors affecting the comparison. The conclusions close the paper.

2 THE ADOPTED PULSATION MODELS

During the last few years, we have been computing an extensive and detailed set of non-linear non-local time-dependent convective models for RR Lyrae stars, spanning a wide range of physical parameters and chemical compositions (see e.g. Bono et al. 2003; Marconi et al. 2003; D04). In this paper, we concentrate on models with metallicity between $Z = 0.0001$ and 0.006, that is the typical range for GGC RR Lyrae. The adopted metallicity, Helium content and stellar parameters are reported in Table 1, whereas the pulsation properties of these models in the Johnson–Cousins bands, as obtained by adopting the static model atmospheres by Castelli, Gratton & Kurucz (1997), as well as an extensive comparison with observed RR Lyrae, are discussed in our previous papers (see e.g. D04; Bono et al. 1997, 2003; Marconi et al. 2003). In particular, D04 discuss in detail the dependence of pulsation properties on the adopted mixing length parameter ($\alpha = l/H_p$ where l is the mixing length and H_p the pressure height scale) that enters the turbolent-convective model to close the non-linear system of dynamical and convective equations (see Bono & Stellingwerf 1994). From this analysis, the authors conclude that the standard value ($\alpha = 1.5$), adopted in all their previous investigations, well reproduces the behaviour of RR Lyrae in the blue regions of the instability strip, whereas there are indications for an increasing α value (up to 2.0) as one moves towards the red edge. In this paper, we concentrate on the models computed with $\alpha = 1.5$ and the stellar parameters reported in Table 1, but we will mention the effect, if any, of a possible alpha increase.

[1]These are the filters that will be mounted on the VST.

3 TRANSFORMATION INTO THE SDSS PHOTOMETRIC SYSTEM

In order to obtain the pulsation observables of the investigated RR Lyrae models in the SDSS bands, we have transformed both the individual static luminosities and effective temperatures and the predicted bolometric light curves into the corresponding filters, by adopting a modified version of a transformation code originally developed by P. G. Prada Moroni (private communication). In particular, as the adoption of linear transformations from one photometric system to another introduces uncertainties (limited precision and strong dependence on the colour range), we directly build magnitudes and colours for our RR Lyrae models by convolving model atmosphere fluxes with SDSS transmission functions.[2] In general, the calculation of the magnitudes in a given photometric system (see e.g. Girardi et al. 2002) involves the integral equation

$$m_{S_\lambda} = -2.5 \log \left(\frac{\int_{\lambda_1}^{\lambda_2} \lambda f_\lambda S_\lambda \, d\lambda}{\int_{\lambda_1}^{\lambda_2} \lambda f_\lambda^0 S_\lambda \, d\lambda} \right) + m_0, \quad (1)$$

where S_λ is the transmission function, f_λ is the stellar flux (that corresponds to model atmospheres of known ($T_{\rm eff}$, $[M/H]$, $\log g$), f_λ^0 is the zero-point reference flux and m_0 is the zero-point reference magnitude. Then, the final absolute magnitudes are computed by the knowledge of the stellar radius.

In the SDSS photometric system (an ABmag system), $m_0 = 0$ and the zero-point reference spectrum is the absolute flux of Vega at 5480 A (Fukugita 1996).

As for model atmospheres, in this paper we adopt the homogeneous set of updated ATLAS9 Kurucz model atmospheres and synthetic fluxes (new-ODF models)[3] computed with a new set of Opacity Distribution Functions (Castelli & Kurucz 2003). These calculations assume steady-state plane-parallel layer atmospheres, covering a metallicity range $[M/H]$: 0.5, 0.2, 0.0, − 0.5, − 1.0, − 1.5, − 2.0 and −2.5, both for $[\alpha/{\rm Fe}] = 0.0$ and for $[\alpha/{\rm Fe}] = 0.4$, temperatures between 3500 and 50 000 K and $\log g$ from 0.0 to 5.0. The Kurucz (1990) model atmospheres had some recognized problems, in particular for effective temperatures lower than 4500 K. One of the reasons was the lack of H_2 O in the line opacity calculations and the use of approximate line data for TiO and CN. The ATLAS9 grids of the new-ODF models were computed with updated solar abundances from Grevesse & Sauval (1998) and considering molecular line lists which include H_2 O molecular transitions and updated TiO and CN data. A comparison between broad-band synthetic colours for late-type giants computed from the new-ODF models and from the PHOENIX/NextGen models has shown a remarkable agreement (Kucinskas et al. 2005, 2006) in spite of the PHOENIX/NextGen models being computed with more molecular species than in ATLAS9 and by assuming spherical simmetry. This last hypothesis is very important when the extent of the atmosphere is comparable with the radius of the star. RR Lyrae stars generally have temperatures higher than 4000 K, however, as a sanity check, for selected models we also computed magnitudes and colours by convolving

[2]The SDSS transmission curves are available at http://www.sdss.org/dr3/instruments/imager/index.html.

[3]Available at http://kurucz.harvard.edu/grids.html or http://wwwuser.oat.ts.astro.it/castelli/grids.html.

the light curves with the PHOENIX/NextGen synthetic spectra[4] (see Section 5).

4 THE PULSATION OBSERVABLES IN THE SDSS PHOTOMETRIC SYSTEM

The application of the procedure discussed in the previous section allows us to predict the pulsation observables and their behaviour as a function of the model input parameters in the SDSS filters. In the following, we explore in detail the morphological features of light curves and the behaviour of mean magnitudes and colours, the topology of the instability strip and colour–colour loops, as well as the main relations between the periods (and the amplitudes) of pulsation and the intrinsic stellar parameters.

4.1 The light curves

All the computed bolometric light curves have been transformed into the SDSS bands.[5] Figs 1–3 show the transformed light curves for both fundamental (F) and first overtone (FO) pulsators at selected luminosity levels and $Z = 0.0001, 0.001$ and 0.006.

As already found for the Johnson–Cousins bands, the pulsation amplitudes vary with the wavelength, increasing from *u* to *g* and decreasing from *g* to *z*. Moreover, for a fixed filter, the amplitudes of fundamental pulsators decrease from the blue to the red edge, whereas the FO ones increase moving from the blue edge to the middle of the instability strip and decrease as the red edge is approached. The agreement between these predicted trends and the observed behaviour of both fundamental and FO pulsators has been extensively discussed in previous papers (see e.g. the discussion in Brocato, Castellani & Ripepi 1996; Bono et al. 1997). We also note that the theoretical light curves in the Johnson–Cousins bands have been successfully compared with available data in the literature (see Bono, Castellani & Marconi 2000; Marconi & Clementini 2005). Unfortunately, a similar comparison cannot be performed for the SDSS filters because of the lack of well-sampled RR Lyrae light curves in these bands.

4.2 The mean magnitudes and colours

From the obtained *u, g, r, i, z* light curves, we can derive mean magnitudes and colours, following different averaging procedures to produce either magnitude-averaged or intensity-averaged values. As already discussed extensively for the Johnson–Cousins bands (see D04), the various types of mean values differ from the static ones the stars would have if they were not pulsating. In Figs 4–5, we show (for F and FO models, respectively) the difference between magnitude-averaged and intensity-averaged mean magnitudes for the *u, g, r, i, z* filters (top panels), as well as the differences between the two kinds of mean values and the corresponding static quantities (middle and bottom panels).

We note that similarly to what happens for the Johnson–Cousins filters, the difference between magnitude-averaged and intensity-averaged magnitudes increases as the corresponding pulsation amplitude increases, reaching the highest values in the *u* and *g* bands.

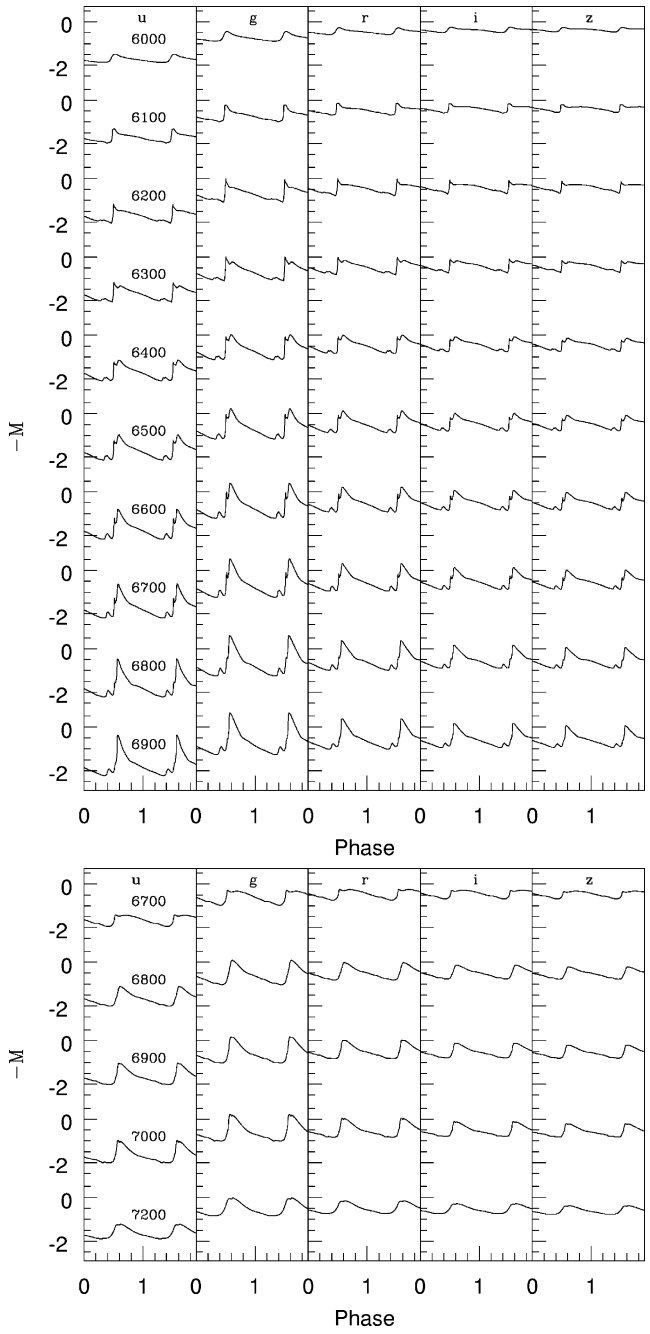

Figure 1. Light curves transformed in the labelled SDSS band for a number of selected F (top) and FO models (bottom) with $Z = 0.0001, M = 0.75\,M_{\odot}$, $\log L/\log L_{\odot} = 1.72$ at varying effective temperature,

Moreover, we confirm that intensity-averaged magnitudes better reproduce the behaviour of static values than the magnitude-averaged ones. Indeed, the difference between the latter mean values and the static ones can reach 0.2 mag in the *g* band. For this reason in the following, we will adopt the intensity-averaged mean magnitudes in the *u, g, r, i, z* filters. These quantities are reported in Tables 2 and 3 for the whole fundamental and FO model sets, respectively.[6]

[4]Available at the web site ftp://ftp.hs.uni-hamburg.de/pub/outgoing/phoenix/GAIA/.

[5]The full set of transformed light curves is available upon request to the authors.

[6]Similar tables for magnitude-averaged values are available upon request to the authors.

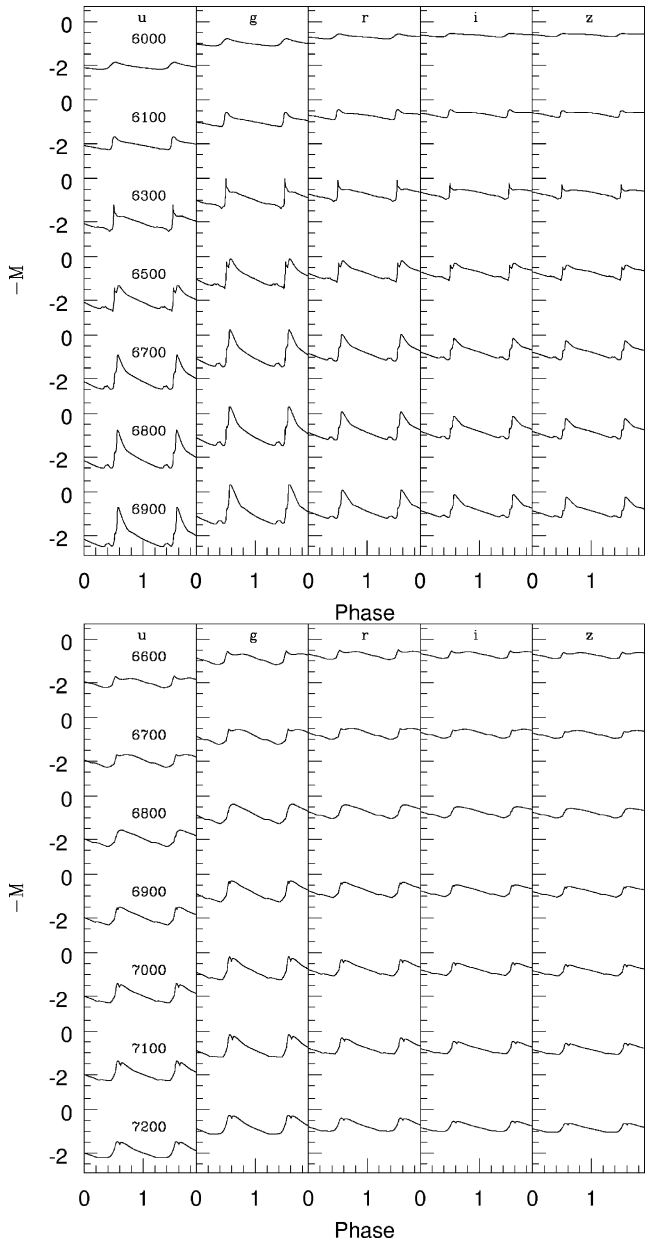

Figure 2. Predicted SDSS light curves for selected F (top) and FO (bottom) models with $Z = 0.001$, $M = 0.65\,\mathrm{M}_{\odot}$, $\log L/\log\,\mathrm{L}_{\odot} = 1.61$ and varying effective temperature.

4.3 The instability strip boundaries

In Fig. 6, we show the predicted instability strip boundaries for both fundamental (solid lines) and FO (dashed lines) models in the intensity-averaged g versus $g - r$ plane, for the metal abundances labelled in different panels. From left to right-hand side, the different lines indicate the first overtone blue edge (FOBE), the fundamental blue edge (FBE), the first overtone red edge (FORE) and the fundamental red edge (FRE). At each magnitude level blue (red) boundaries correspond to the effective temperatures of the first (last) pulsating model in the selected mode. Concerning the behaviour of the boundaries in the magnitude–period diagram, a linear regression to all the models quoted in Table 1 yields, by taking into account the first (for the FOBE) and the last (for the FRE) pulsating models, the mass-dependent analytical relations reported in Table 4. The

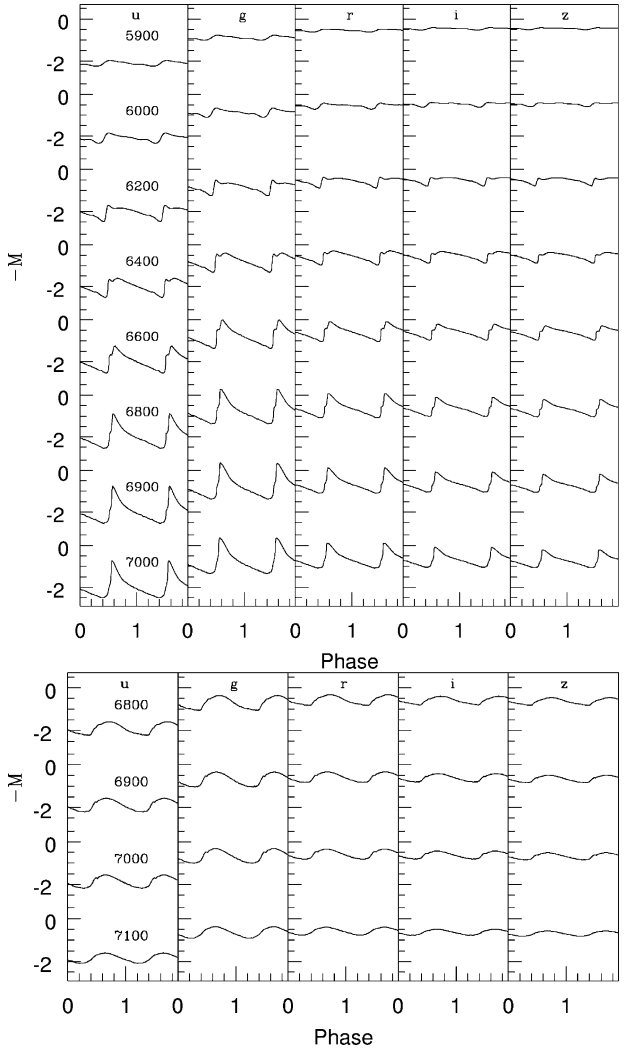

Figure 3. Predicted SDSS light curves for selected F (top) and FO (bottom) models with $Z = 0.006$, $M = 0.58\,\mathrm{M}_{\odot}$, $\log L/\log\,\mathrm{L}_{\odot} = 1.65$ and varying effective temperature.

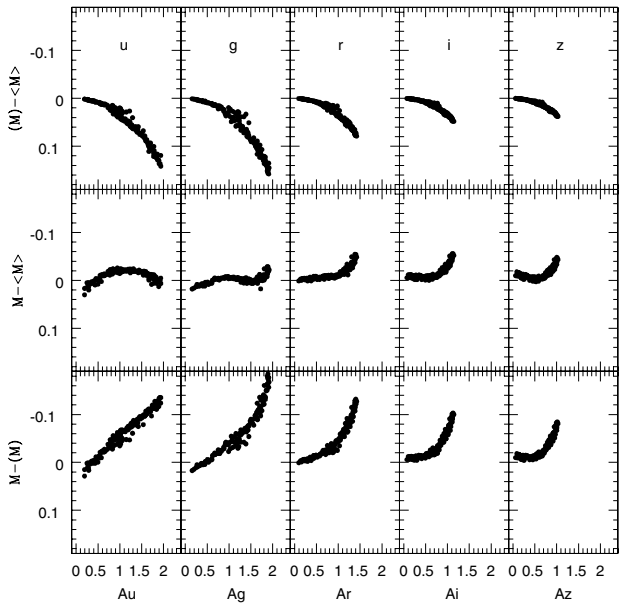

Figure 4. Comparison between static and mean magnitudes for F models.

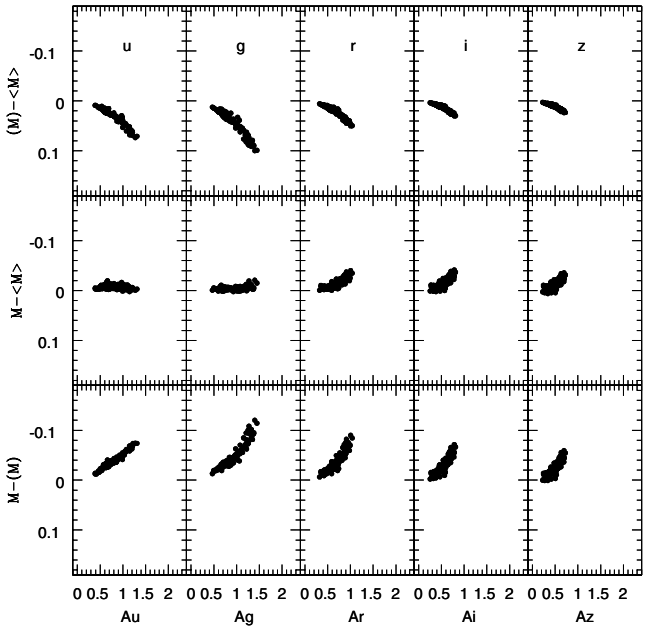

Figure 5. The same as the previous figure but for FO models.

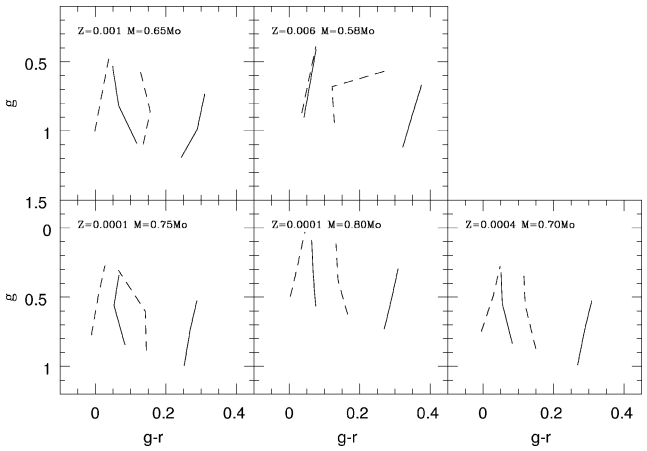

Figure 6. Predicted instability strip boundaries for both F (solid lines) and FO (dashed lines) models in the intensity-averaged g versus $g-r$ plane. The adopted metal abundances and stellar masses are labelled.

Table 4. Analytical relations for the FOBE and FRE in the form $M_i = a + b\log P + c\log\frac{M}{M_\odot} + d\log Z$. The dispersion σ (mag) is also reported.

M_i	Boundary	a	b	c	d	σ
u	FOBE	0.40	−2.32	−1.95	0.086	0.03
	FRE	1.64	−1.79	−2.43	0.12	0.03
g	FOBE	−1.04	−2.43	−2.14		0.04
	FRE	0.18	−1.99	−2.34		0.02
r	FOBE	−1.12	2.63	−1.85		0.03
	FRE	−0.07	−2.23	−1.92		0.02
i	FOBE	−1.11	−2.72	−1.86		0.03
	FRE	−0.18	−2.34	−1.96		0.01
z	FOBE	−1.09	−2.78	−1.91		0.02
	FRE	−0.22	−2.40	−2.05		0.01

zero point of the FOBE relation varies by ∼0.08 mag in g and by ∼0.06 mag in i if the assumed α value increases from 1.5 to 2.0. The corresponding zero-point variation for the FRE is ∼0.3 mag in g and ∼0.01 mag in i (see also the discussion in D04).

Only for the u filter, we also find a non-negligible dependence on the metal content and in all cases the standard deviations are of the order of a few hundredth of magnitude.

4.4 The colour–colour loops

The transformed multifilter light curves can be reported in different colour–colour planes. In Figs 7–9, we show the theoretical loops in the $g-r$ versus $u-g, r-i$ versus $g-r$ and $i-z$ versus $r-i$ diagrams for selected models (see Table 5) at each adopted metallicity. We note that the metallicity effect is more evident in Fig. 7 due to the significant sensitivity of the u band on metal abundance. On the other hand, in the $r-i$ versus $g-r$ plane the loops are very narrow and the effect of metallicity is smaller, so that, once the metallicity is known, the comparison between theory and observations in this plane could be used to evaluate colour excesses. As for the $i-z$ versus $r-i$ diagram, the predicted loops are very close to each other and the metallicity dependence is much less evident than for the other colour combinations. A linear regression through the intensity-averaged mean magnitudes reported in Tables 2 and 3 provides the following metal-dependent analytical colour–colour relations:

$$u-g = 1.41 - 0.12(g-r) + 0.088\log Z \quad (\sigma = 0.03)$$
$$g-r = 0.234 + 2.11(r-i) + 0.035\log Z \quad (\sigma = 0.006)$$
$$r-i = 0.085 + 2.04(i-z) + 0.0097\log Z \quad (\sigma = 0.004) \qquad (2)$$

Table 2. Intensity-averaged mean magnitudes for the full set of fundamental models (the full table is available in the electronic form).

Z	$M/M_\odot$	$\log L/\log L_\odot$	T_e (K)	P (d)	$\langle u\rangle$	$\langle g\rangle$	$\langle r\rangle$	$\langle i\rangle$	$\langle z\rangle$
0.0001	0.65	1.61	6900	0.4059	1.8978	0.8378	0.7813	0.8054	0.8419
0.0001	0.65	1.61	6800	0.4260	1.9090	0.8445	0.7675	0.7808	0.8118
...	...	...	...	...	...	....	...	...	...

Table 3. Intensity-averaged mean magnitudes for the full set of FO models (the full table is available in the electronic form).

Z	$M/M_\odot$	$\log L/\log L_\odot$	T_e (K)	P (d)	$\langle u\rangle$	$\langle g\rangle$	$\langle r\rangle$	$\langle i\rangle$	$\langle z\rangle$
0.0001	0.65	1.61	7300	0.2527	1.8838	0.7553	0.7572	0.8255	0.8918
0.0001	0.65	1.61	7200	0.2634	1.8843	0.7737	0.7664	0.8242	0.8826
...	...	...	...	...	...	....	...	...	...

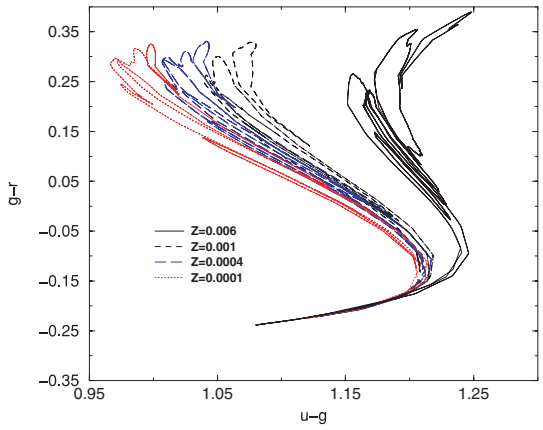

Figure 7. Theoretical loops in the $g - r$ versus $u - g$ diagram for selected models (see Table 5) at each adopted metallicity.

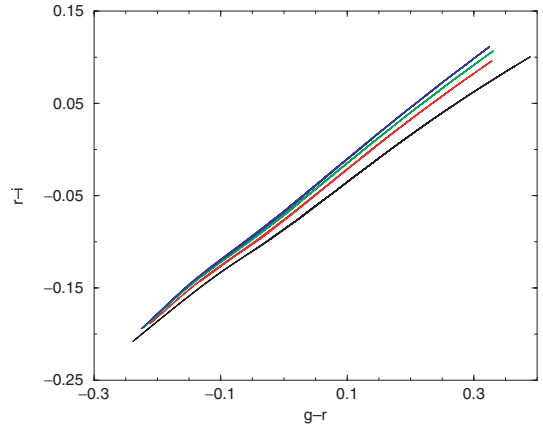

Figure 8. The same as in Fig. 7 but in the $r - i$ versus $g - r$ diagram; in this plane the loops move upwards as the metallicity decreases.

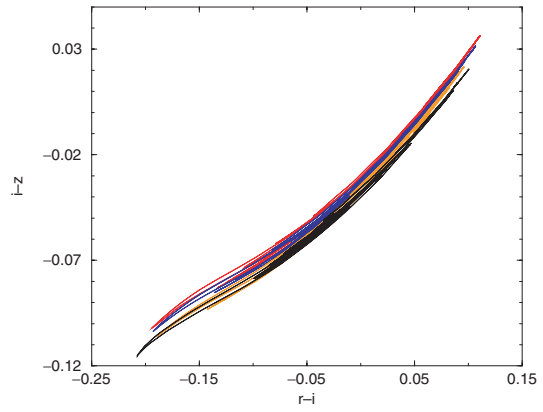

Figure 9. The same as in Fig. 7 but in the $i - z$ versus $r - i$ diagram.

holding for fundamental pulsators, and

$$u - g = 1.35 - 0.19(g - r) + 0.065 \log Z \quad (\sigma = 0.02)$$
$$g - r = 0.217 + 1.95(r - i) + 0.0258 \log Z \quad (\sigma = 0.006)$$
$$r - i = 0.082 + 2.00(i - z) + 0.0062 \log Z \quad (\sigma = 0.003) \qquad (3)$$

for the FO ones.

Table 5. Physical parameters of models plotted in the colour–colour diagrams.

Z	Y	$M/\mathrm{M}_\odot$	$\log L/\log \mathrm{L}_\odot$	T_e	Mode
0.0001	0.24	0.80	1.81	7100	FO
0.0001	0.24	0.80	1.81	6800	FO
0.0001	0.24	0.80	1.81	6700	F
0.0001	0.24	0.80	1.81	6300	F
0.0001	0.24	0.80	1.81	5900	F
0.0004	0.24	0.70	1.72	7000	FO
0.0004	0.24	0.70	1.72	6700	FO
0.0004	0.24	0.70	1.72	6700	F
0.0004	0.24	0.70	1.72	6400	F
0.0004	0.24	0.70	1.72	5950	F
0.001	0.24	0.65	1.61	7200	FO
0.001	0.24	0.65	1.61	6800	FO
0.001	0.24	0.65	1.61	6700	F
0.001	0.24	0.65	1.61	6400	F
0.001	0.24	0.65	1.61	6100	F
0.006	0.26	0.58	1.65	7100	FO
0.006	0.26	0.58	1.65	6900	FO
0.006	0.26	0.58	1.65	6800	FO
0.006	0.26	0.58	1.65	7000	F
0.006	0.26	0.58	1.65	6400	F
0.006	0.26	0.58	1.65	6000	F

4.5 The multifilter period–magnitude–colour relations

The obvious outcome of the pulsation relation (see Van Albada & Baker 1971; D04) connecting the period to the mass, the luminosity and the effective temperature into the observational plane is the period–magnitude–colour (PMC) relation, where the pulsation period for each given mass is correlated with the pulsator absolute magnitude and colour. A linear regression through the intensity-averaged values reported in Tables 2 and 3 provides a PMC relation for each selected couple of bands and chemical composition.

In particular, we find

$$u = 6.43 - 0.89 \log P - 3.78(u - g) - 2.84 \log M + 0.36 \log Z$$
$$\sigma = 0.14 \qquad (4)$$

$$g = -1.05 - 2.87 \log P + 3.35(g - r) - 1.87 \log M - 0.06 \log Z$$
$$\sigma = 0.02 \qquad (5)$$

$$g = -0.83 - 2.87 \log P + 2.27(g - i) - 1.94 \log M - 0.024 \log Z$$
$$\sigma = 0.02 \qquad (6)$$

$$g = -0.67 - 2.91 \log P + 1.99(g - z) - 1.90 \log M$$
$$\sigma = 0.07 \qquad (7)$$

for fundamental models and

$$u = 5.77 - 1.48 \log P - 3.87(u - g) - 2.72 \log M + 0.25 \log Z$$
$$\sigma = 0.07 \qquad (8)$$

$$g = -1.53 - 3.11 \log P + 3.57(g - r) - 1.63 \log M - 0.042 \log Z$$
$$\sigma = 0.01 \qquad (9)$$

$$g = -1.279 - 3.07 \log P + 2.334(g - i) - 1.72 \log M - 0.017 \log Z$$
$$\sigma = 0.009 \qquad (10)$$

Table 6. Pulsation amplitudes for the full set of fundamental models (the full table is available in the electronic form).

Z	$M/M_\odot$	$\log L/\log L_\odot$	T_e (K)	P (d)	A_u	A_g	A_r	A_i	A_z
0.0001	0.65	1.61	6900	0.4059	1.7877	1.8675	1.3689	1.0900	0.9669
0.0001	0.65	1.61	6800	0.4260	1.6424	1.7906	1.2955	1.0261	0.9187
...	...	...	...	...	...	....	...	...	...

Table 7. Pulsation amplitudes for the full set of FO models (the full table is available in the electronic form).

Z	$M/M_\odot$	$\log L/\log L_\odot$	T_e (K)	P (d)	A_u	A_g	A_r	A_i	A_z
0.0001	0.65	1.61	7300	0.2527	0.3939	0.4978	0.3522	0.2727	0.2427
0.0001	0.65	1.61	7200	0.2634	0.9037	1.0765	0.7677	0.5969	0.5296
...	...	...	...	...	...	....	...	...	...

$$g = -1.151 - 3.099 \log P + 2.02(g-z) - 1.77 \log M - 0.0045 \log Z$$
$$\sigma = 0.007 \qquad (11)$$

for the FO ones. As discussed in D04 for the Johnson–Cousins bands, these relations allow us to derive an estimate of the stellar mass for RR Lyrae of known distance and colour, while for cluster pulsators sharing the same distance and reddening, they provide direct estimates of the mass spread. On the other hand, if the mass and colours are known, the same relations can be used to infer individual and/or mean distance moduli of RR Lyrae stars in a given globular cluster or galaxy.

4.6 The pulsation amplitudes

The pulsation amplitudes of the fundamental and FO multiwavelength light curves are reported in Tables 6 and 7. Their behaviour as a function of the pulsation period is shown in Fig. 10 for selected model sequences at $Z = 0.0001$ (left-hand panels) and $Z = 0.001$ (right-hand panels). We note that the fundamental pulsators follow a linear behaviour, thus allowing the derivation of a mass-dependent linear relation between the period, the pulsation amplitude and the absolute magnitude. The coefficients of these relations for the whole fundamental model set and the various photometric bands are reported in Table 8. We note that the coefficients of these relations are expected to depend on the adopted α parameter (see also D04). In particular in the g filter, the zero point and the amplitude coefficient should vary by ∼0.14 and ∼0.38, respectively, as α increases from 1.5 to 2.0.

As for FO pulsators, we note the characteristic bell shape also shown in the bolometric and Johnson–Cousins band Bailey diagram (see e.g. Bono et al. 1997). In Figs 11 and 12, we show the amplitude ratios between the Johnson V and the SDSS g bands (left top panel of each figure) and between the u, r, i, z and the g bands,

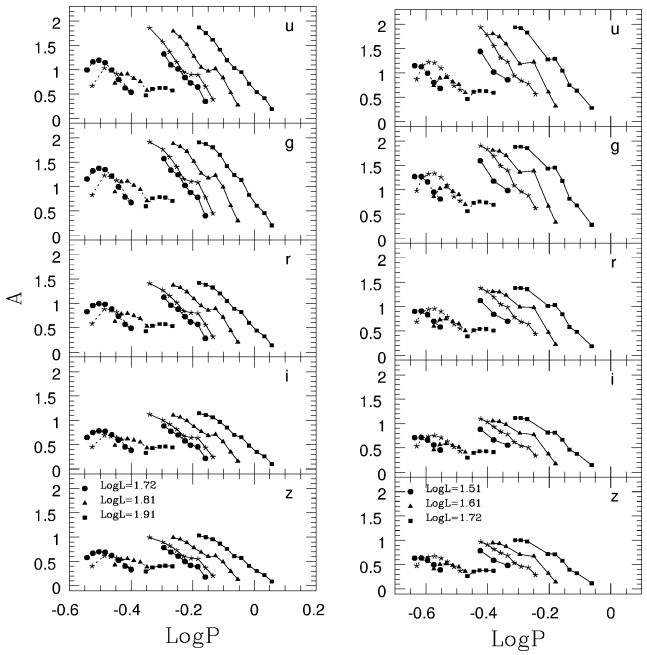

Figure 10. Period–amplitude diagram for FO (dashed line) and F (solid line) models with $M = 080\,M_\odot$ and $Z = 0.0001$ (left-hand panel) and $M = 0.65\,M_\odot$ $Z = 0.001$(right-hand panel) and for the three labelled values of $\log L/\log L_\odot$. In both cases, star symbols represent models with $M = 0.75\,M_\odot$.

Table 8. Analytical coefficients of the period–luminosity–amplitude relations in the form $\log P = a + bA_i + c\langle M_i\rangle + d \log \frac{M}{M_\odot} + e \log Z$.

M_i	a	b	c	d	e	σ
u	0.72	−0.186	−0.41	−0.73	0.038	0.02
g	0.14	−0.184	−0.371	−0.54	0.009	0.02
r	−0.03	−0.174	−0.372	−0.60	−0.015	0.01
i	−0.07	−0.171	−0.370	−0.64	0.069	0.01
z	−0.074	−0.164	−0.368	−0.66	0.074	0.009

for fundamental and FO models, respectively. We note that the g band amplitude is systematically higher than the V amplitude, independent of the period and the adopted metal abundance (see labels). At the same time, the amplitudes in the r, i, z filters scale with a constant mean ratio (ranging from about 0.7 to 0.5 from r to z) with the g band amplitude, thus suggesting that only few points along the light curves in these filters will be required, if the g curve is accurately sampled. As for the u band, the scatter is larger due to the significant dependence on the adopted metallicity. This occurrence is more evident for fundamental models, which are characterized by more asymmetric light curves and higher pulsation amplitudes.

We note that, once known the metal content, the mass term contained in all the analytical relations reported in this section can be replaced with the value predicted by evolutionary horizontal branch

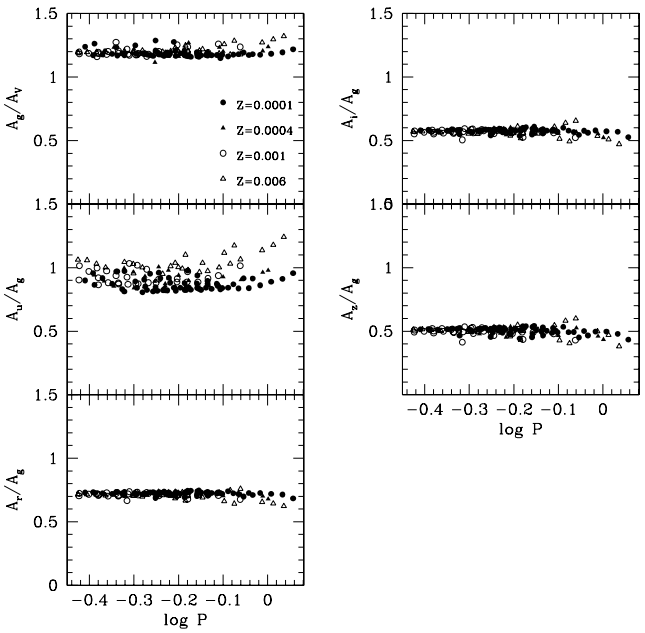

Figure 11. Amplitude ratios between the Johnson V and the SDSS g bands (left top panel) and between the u, r, i, z and the g bands for fundamental models.

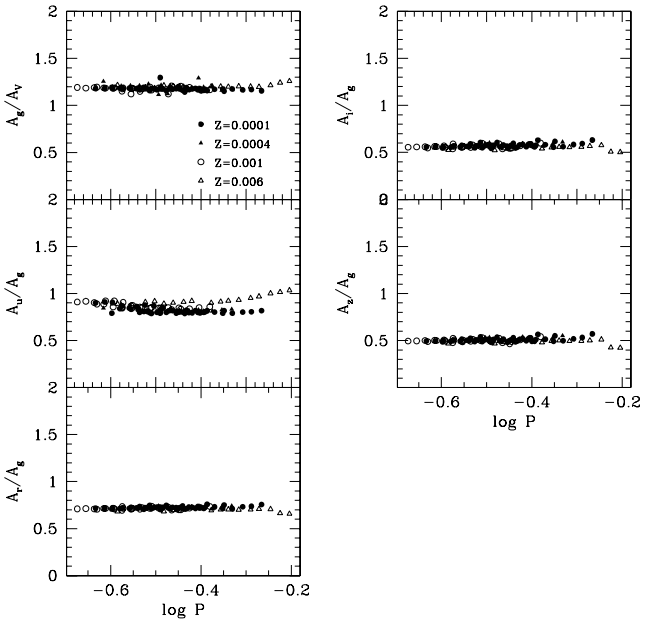

Figure 12. The same as the previous figure but for FO models.

computations at the selected metallicity (see e.g. columns 5 and 6 of table 1 in Bono et al. 2003).

5 COMPARISON WITH THE OBSERVATIONS

In this section, the predicted colour–colour loops in various filter combinations are compared with observed RR Lyrae samples. In particular, we test our predictions with the QUEST survey (see e.g. Vivas et al. 2001) and the observations in the Draco galaxy (Bonanos et al. 2004). The first one, a large census of field RR Lyrae, should map the history of the outer halo of our Galaxy, and

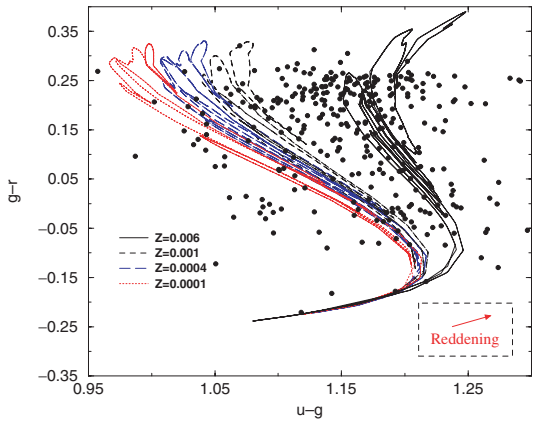

Figure 13. Comparison between the theoretical loops shown in Fig. 7 and the QUEST RR Lyrae data (see text for details).

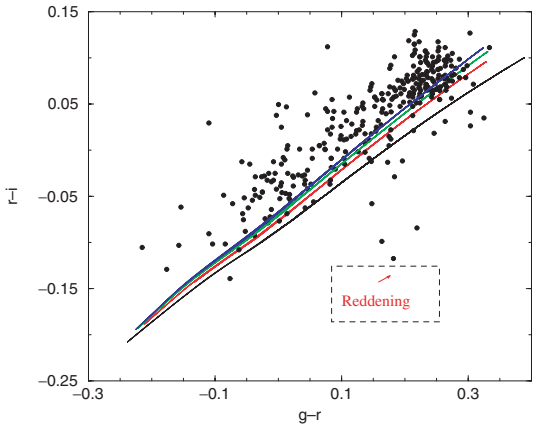

Figure 14. Comparison between the theoretical loops shown in Fig. 8 and the QUEST RR Lyrae data (see text for details).

the second one should represent an example of RR Lyrae in a different environment.

Both the samples are positionally matched against the SDSS-Data Release four (DR4) (Adelman-McCarthy et al. 2006) catalogue using a search radius of 0.1 arcsec and subsequently dereddened [using infrared (IR) maps; see Schlegel, Finkbeiner & Davis 1998]. Figs 13 and 14 show the distributions for QUEST data, as observed in the $g - r$ versus $u - g$ and $r - i$ versus $g - r$ plane, respectively. Superimposed, we show the theoretical loops for the labelled metallicities instead of average values because SDSS observations consist of one or, at the most, two phase points. The QUEST data which are expected to trace metal-poor ($Z < 0.001$) and distant halo stars (see Vivas et al. 2001) are not matched by the corresponding model loops, with the discrepancy larger than the mean uncertainty resulting from photometric [$\sigma\ (u - g) < 0.03$ mag] and reddening errors (less than 0.01 mag in colours; see also Ivezic et al. 2005). In Fig. 15, we show the comparison with Draco RR Lyrae in the $g - r$ versus $u - g$ plane. In this case, we have a large spread in $u - g$ due in part to the significant photometric uncertainties [$\sigma\ (u - g) \sim 0.1$ mag and $\sigma\ (g - r) \sim 0.02$] affecting the data. In this case, the comparison with the theoretical loops does not allow us to discriminate a metallicity effect. However, the mean metallicity of this galaxy is generally considered poorer than $Z = 0.001$ (see e.g. Mateo 1998), thus it is noteworthy that a consistent fraction of the Draco RR Lyare is

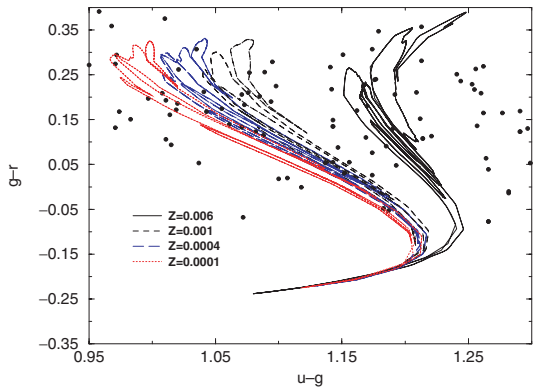

Figure 15. The same as for Fig. 13 but for Draco RR Lyrae.

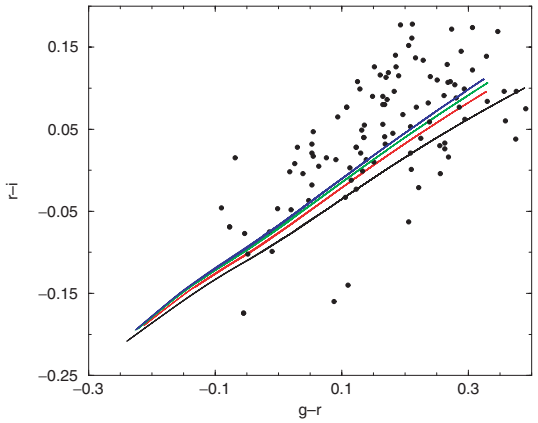

Figure 16. The same as for Fig. 14 but for Draco RR Lyrae.

redder than our $Z = 0.006$ models with an overdensity at $u - g > 1.25$ (difficult to explain with the photometric error alone). The situation is similar in the $r - i$ versus $g - r$ plane (see Fig. 16). Possible sources for the discrepancies between theory and observation may result from observational uncertainties, including reddening and contamination effects, or theoretical biases, as, for example, the adopted model atmospheres and chemical mixture.

As for the reddening, a critical point is represented by the extinction law adopted to relate the measured $E(B - V)$ to the extinctions in the SDSS filters (see e.g. Girardi et al. 2004). Assuming the coefficients tabulated by Girardi et al. (2004), an underestimation of the $E(B - V)$ colour excesses of the order of 0.02 mag would require a redshift in the theoretical $u - g$ and $g - r$ of about 0.03 and 0.02, respectively, in the direction of reducing the discrepancy between data and metal-poor predictions in Figs 13 and 14 (see the arrow in these plots).

Concerning model atmospheres, as discussed in Section 3, we have adopted ATLAS models (Castelli & Kurucz 2003) without α enhancement. In order to explore the effect of possible α enhancement for the lowest metallicities, as empirically suggested by various authors in the literature (see e.g. Gratton et al. 2003), we have transformed again the theoretical bolometric light curves by using ATLAS model atmospheres with $[\alpha/\mathrm{Fe}] = 0.4$ and reducing the adopted [Fe/H] in order to obtain the same global model metallicity (see Salaris, Chieffi & Straniero 1993). As an example, in Fig. 17 we show the variation of the theoretical loops for models with $Z = 0.0004$. It appears that increasing $[\alpha/\mathrm{Fe}]$ from 0 to 0.4 produces a larger discrepancy between metal-poor models and the data. On the

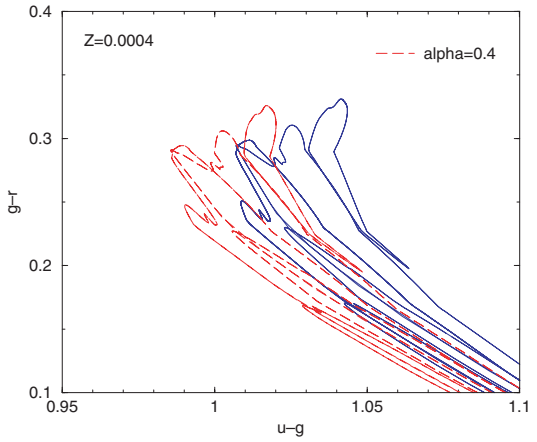

Figure 17. Variation of the theoretical loops in the $g - r$ versus $u - g$ plane for models with $Z = 0.0004$, as the $[\alpha/\mathrm{Fe}]$ increases from 0 to 0.4.

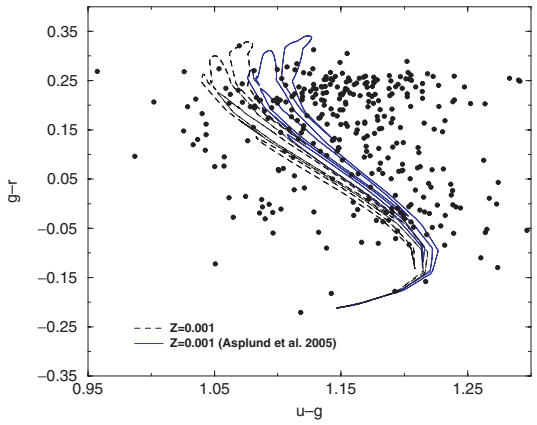

Figure 18. Comparison between the theoretical loops shown in Fig. 7 and the QUEST RR Lyrae data (see text for details).

other hand, if in the conversion from Z to [Fe/H], we replace the assumed solar metallicity with the more updated value by Asplund, Grevesse & Sauval (2005), loops of a given metallicity move redwards by about 0.05 mag in $g - r$ versus $u - g$ plane (see e.g. Fig. 18 for $Z = 0.001$), so that the recovered global metallicity for halo RR Lyare is closer to typical values in the literature.

To take into account the effect of the adopted set of model atmospheres, Fig. 19 plots the same comparison as in Fig. 13 but using the PHOENIX atmospheres for giant stars (Kucinskas et al. 2006), which have the main advantage of assuming the spherical geometry instead of the classical plane-parallel structure. From the $u - g$ versus $g - r$ plot, it is evident that the PHOENIX atmospheres affect the $u - g$ colour with a bluewards shift (of about 0.03 mag) for models with $g - r$ between 0.1 and 0.3 mag, corresponding to the bulk of the observed RR Lyrae. Moreover, the PHOENIX atmospheres lead to redder $u - g$ colours (by about 0.05 mag) for stars with $g - r$ lower than 0.1 mag, where the RR Lyare density is lower. However, both these effects produce minor changes in the behaviour observed in Figs 13 and 14.

6 CONCLUSIONS

We have transformed the predicted scenario for RR Lyrae stars with Z in the range 0.0001–0.006 into the SDSS photometric system,

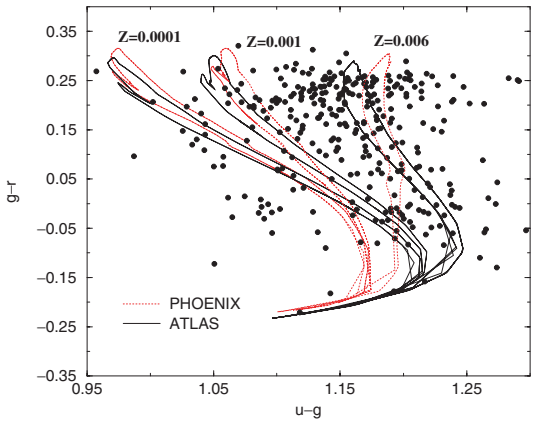

Figure 19. The QUEST RR Lyrae data compared with selected models transformed both with ATLAS (solid lines) and with PHOENIX (dotted lines) model atmospheres.

providing theoretical tools for the interpretation of modern large RR Lyrae surveys in these bands. Mean magnitudes and colours and the pulsation amplitudes are used to derive multiband analytical relations that can be used to constrain both the distances and the stellar masses. Rather constant amplitude ratios are found for *r, i, z* with respect to the *g* band, suggesting that only few points along the light curves in these filters will be required, if the *g* curve is accurately sampled. The theoretical $g - r$ versus $u - g$ and $r - i$ versus $g - r$ are compared with available data in the literature. In particular, for field RR Lyrae stars from the QUEST survey the comparison seems to suggest a higher mean metallicity than usually assumed. In order to understand this occurrence, several sources of systematic errors have been discussed.

ACKNOWLEDGMENTS

We thank P. G. Prada Moroni and S. Degl'Innocenti for useful comments and suggestions on filter transformations. Financial support for this study was provided by MIUR, under the scientific project 'on the evolution of stellar systems: fundamental step toward the scientific exploitation of VST' (P.I. Massimo Capaccioli). This project made use of computational resources granted by the 'Consorzio di Ricerca del Gran Sasso' according to the 'Progetto 6: Calcolo Evoluto e sue applicazioni (RSV6) – Cluster C11/B'.

REFERENCES

Adelman-McCarthy J. K. et al., 2006, ApJS, 162, 38
Alcalá J. M. et al., 2006, Mem. della Soc. Astron. Ital. Supp., 9, 204
Asplund M., Grevesse N., Sauval A. J., 2005, in Bash F. N., Barnes T. J., eds, ASP Conf. Ser. Vol. 336, Cosmic Abundances as Records of Stellar Evolution and Nucleosynthesis. Astron. Soc. Pac., San Francisco, p. 25
Bonanos A. Z., Stanek K. Z., Szentgyorgyi A. H., Sasselov D. D., Bakos G. A., 2004, AJ, 127, 861
Bono G., Stellingwerf R. F., 1994, ApJS, 93, 233
Bono G., Caputo F., Castellani V., Marconi M., 1997, A&AS, 121, 327
Bono G., Castellani V., Marconi M., 2000, ApJ, 532, L129
Bono G., Caputo F., Castellani V., Marconi M., Storm J., Degl'Innocenti S., 2003, MNRAS, 344, 1097
Brocato E., Castellani V., Ripepi V., 1996, AJ, 111, 809
Brown T. M., Ferguson H. C., Smith E., Kimble R. A., Sweigart A. V., Renzini A., Rich R. M., 2004, AJ, 127, 2738
Cacciari C., 2003, in Piotto G., Meylan G., Djorgovski S. G., Riello M., eds, ASP Conf. Ser. Vol. 296, New Horizons in Globular Cluster Astronomy. Astron. Soc. Pac., San Francisco, p. 329
Caputo F., Castellani V., Marconi M., Ripepi V., 2000, MNRAS, 316, 819
Castelli F., Kurucz R. L., 2003, in Piskunov N. E., Weiss W. W., Gray D. F., eds, IAU Symp. 210, Modelling of Stellar Atmospheres. Astron. Soc. Pac., San Francisco
Castelli F., Gratton R. G., Kurucz R. L., 1997, A&A, 318, 841
Di Criscienzo M., Marconi M., Caputo F., 2004, ApJ, 612, 1092 (D04)
Di Criscienzo M., Caputo F., Marconi M., Musella I., 2006, MNRAS, 365, 1357
Dinescu D. I., Keeney B. A., Majewski S. R., Girard T. M., 2004, AJ, 128, 687
Fukugita M., Ichikawa T., Gunn J. E., Doi M., Shimasaku K., Schneider D. P., 1996, AJ, 111, 1748
Girardi L., Bertelli G., Bressan A., Chiosi C., Groenewegen M. A. T., Marigo P., Salasnich B., Weiss A., 2002, A&A, 391, 195
Girardi L., Grebel E. K., Odenkirchen M., Chiosi C., 2004, A&A, 422, 205
Gratton R. G., Carretta E., Desidera S., Lucatello S., Mazzei P., Barbieri M., 2003, A&A, 406, 131
Grevesse N., Sauval A. J., 1998, Space Sci. Rev., 85, 161
Ivezic Z. et al., 2000, AJ, 120, 963
Ivezic Z., Vivas A. K., Lupton R. H., Zinn R., 2005, AJ, 129, 1096
Kucinskas A., Hauschildt P. H., Ludwig H. G., Brott I., Vansevicius V., Lindegren L., Tanabé T., Allard F., 2005, A&A, 442, 281
Kucinskas A., Hauschildt P. H., Brott I., Vansevicius V., Lindegren L., Tanabé T., Allard F., 2006, A&A, 452, 1021
Kurucz R. L., 1990, in Crivellari L. et al., eds, Stellar Atmospheres: Beyond Classical Models, NATO Asi Ser., p. 441
Lynden-Bell D., 1982, Observatory, 102, 202
Marconi M., Clementini G., 2005, AJ, 129, 2257
Marconi M., Caputo F., Di Criscienzo M., Castellani M., 2003, ApJ, 596, 299
Marconi M. et al., 2006, Mem. della Soc. Astron. Ital. Supp., 9, 253
Mateo M. L., 1998, ARA&A, 36, 435
Salaris M., Chieffi A., Straniero O., 1993, ApJ, 414, 580
Schlegel D. J., Finkbeiner D. P., Davis M. 1998, ApJ, 500, 525
Van Albada T. S., Baker N., 1971, ApJ, 169, 311
Vivas A. K., Zinn R., 2006, AJ, 132, 714
Vivas A. K. et al., 2001, ApJ, 554, 33
Vivas A. K. et al., 2004, AJ, 127, 1158
Wu C., Qiu Y. L., Deng J. S., Hu J. Y., Zhao Y. H., 2005, AJ, 130, 1640

SUPPLEMENTARY MATERIAL

The following supplementary material is available for this article online.

Table 2. Intensity-averaged mean magnitudes for the full set of fundamental models.

Table 3. Intensity-averaged mean magnitudes for the full set of first-overtone models.

Table 6. Pulsation amplitudes for the full set of fundamental models.

Table 7. Pulsation amplitudes for the full set of first-overtone models.

This material is available as part of the online article from http:www.blackwell-synergy.com.

This paper has been typeset from a TEX/LATEX file prepared by the author.